

# Large-aperture prism-array lens for high-energy X-ray focusing

Weiwei Zhang,<sup>a</sup> Jing Liu,<sup>a\*</sup> Guangcai Chang,<sup>a\*</sup> Zhan Shi,<sup>a</sup> Ming Li,<sup>a</sup> Yuqi Ren,<sup>b</sup> Xiaowei Zhang,<sup>a</sup> Futing Yi,<sup>a</sup> Peng Liu<sup>a</sup> and Weifan Sheng<sup>a</sup>

<sup>a</sup>Beijing Synchrotron Radiation Facility, Institute of High Energy Physics, Chinese Academy of Sciences, Beijing 100049, People's Republic of China, and <sup>b</sup>Shanghai Synchrotron Radiation Facility, Shanghai Institute of Applied Physics, Chinese Academy of Sciences, Shanghai 201204, People's Republic of China.

\*Correspondence e-mail: liujing1987@ihep.ac.cn, changgc@ihep.ac.cn

Received 26 April 2016

Accepted 8 July 2016

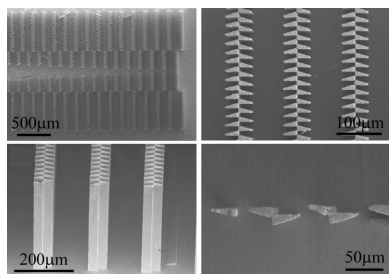
Edited by S. M. Heald, Argonne National Laboratory, USA

**Keywords:** X-ray optics; refractive lenses; prism-array lenses; LIGA technology; knife-scan method.

A new prism-array lens for high-energy X-ray focusing has been constructed using an array of different prisms obtained from different parabolic structures by removal of passive parts of material leading to a multiple of  $2\pi$  phase variation. Under the thin-lens approximation the phase changes caused by this lens for a plane wave are exactly the same as those caused by a parabolic lens without any additional corrections when they have the same focal length, which will provide good focusing; at the same time, the total transmission and effective aperture of this lens are both larger than those of a compound kinoform lens with the same focal length, geometrical aperture and feature size. This geometry can have a large aperture that is not limited by the feature size of the lens. Prototype nickel lenses with an aperture of 1.77 mm and focal length of 3 m were fabricated by LIGA technology, and were tested using CCD camera and knife-edge scan method at the X-ray Imaging and Biomedical Application Beamline BL13W1 at Shanghai Synchrotron Radiation Facility, and provided a focal width of 7.7  $\mu\text{m}$  and a photon flux gain of 14 at an X-ray energy of 50 keV.

## 1. Introduction

X-ray refractive lenses have created their own space in X-ray focusing after being demonstrated by Snigirev *et al.* in 1996 (Snigirev *et al.*, 1996). However, this kind of lens also has substantial limitations arising from a noticeable decrease of radiation intensity along the beam trajectory and quite tiny refraction. The weak refractive effect is overcome by stacking a large number of lenses in series, known as a compound refractive lens (CRL) (Snigirev *et al.*, 1996, 1998; Lengeler *et al.*, 2001; Schroer *et al.*, 2003), while the most radical way to overcome the limitation connected with the loss of radiation is the development of special kinoform lenses (KLs, also known as Fresnel-like lenses), which are realised by removing passive parts of material where the phase variation is a multiple of  $2\pi$  and are composed of a series of tooth-like segments (Aristov *et al.*, 2000; Evans-Lutterodt *et al.*, 2003, 2007). In these typical KLs, the tooth-like structures in the middle are sparse and have large widths, while those further away from the middle are dense and have smaller widths. Actually, the aperture of a KL is strongly limited by its fabrication challenges, as the feature size (*e.g.* width) of the tooth-like segments on two sides are smaller and smaller which becomes difficult to fabricate. To avoid the inconvenience of the fabrication of small tooth-like segments of KLs, prism-array lenses composed of identical triangle structures of the same width were first proposed by Jark *et al.* (2004), and a simple correction was applied to the outermost prism side-walls to



realise ideal focusing. Cederström *et al.* (2005) presented a more general modification of the multi-prism lens and quasi-parabolic profiles were obtained. Prism-array lenses have fewer segments in the middle but more at the two sides, and were shown to efficiently refract X-rays as expected (Jark *et al.*, 2004; Cederström *et al.*, 2005; Simon *et al.*, 2008; Nazmov *et al.*, 2013).

In this paper we propose a new design of prism-array lens (PL) with large aperture for high-energy X-ray focusing, which differs from those mentioned above. It is not composed of identical triangles but of different parabolic elements obtained from different parabolic profiles. Under the thin-lens approximation, the phase changes caused by a PL for a plane wave are exactly the same as those caused by a parabolic refractive lens (PRL) or a KL without any additional corrections when they have the same focal length. This geometry can have a large aperture that is not limited by the feature size of the lens and will provide good focusing for high-energy X-rays.

## 2. Theory

### 2.1. Design

KLs are formed by removing excessive material from one parabolic profile refractive lens, while PLs are obtained from different parabolic profiles, as shown in Fig. 1(a) (the thin-lens approximation and only one-dimensional focusing are considered). The width of a tooth-like segment is  $\Delta r(n, m)$ , where  $n$  is the order of different parabolic profiles and  $m$  is the

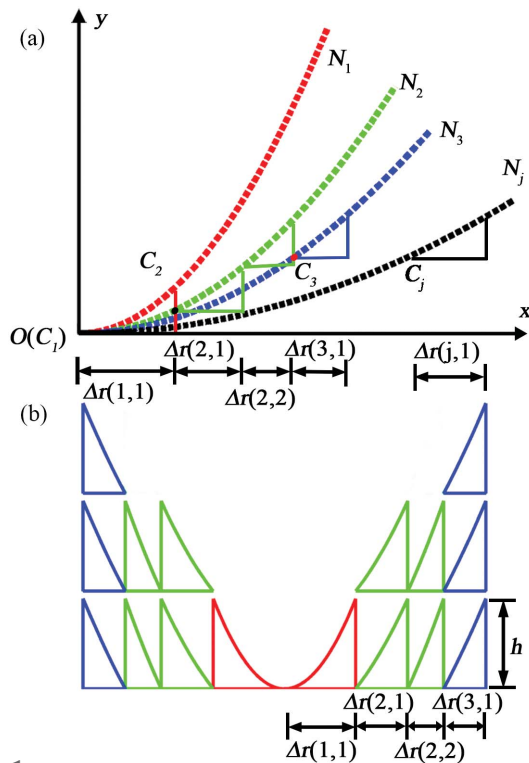


**Figure 1**  
The derivation of a PL from different parabolic profiles. The tooth-like segments with the same colour are obtained from the same parabolic profiles. (An example:  $n_1 = 1, n_2 = 2, n_3 = 1; N_1 = 1, N_2 = 2, N_3 = 3$ .)

order of tooth-like segments obtained from the same parabolic profile. The height of the tooth-like segment is  $h$ , and  $h = \lambda/\delta$ , corresponding to the  $2\pi$  phase change, where  $\delta$  is the refraction index decrement. We assume that the smallest  $\Delta r(n, m)$  is  $\Delta$ , which can be successfully fabricated within the tolerance of the state-of-the-art production technology, and the desired focal length of the lens is  $f$ . The profile of a PRL with focal length  $f$  is

$$y = x^2/(2\delta f), \quad (1)$$

while for a compound refractive lens with number  $N$  and focal length  $f$  the focal length of each single lens is  $f/N$  and the profile of each single lens is

$$y = x^2/(2\delta fN). \quad (2)$$

First, let  $N = 1$ , then the lens profile is  $y_1 = x^2/(2\delta f \times 1)$ . Then material leading to a multiple of  $2\pi$  phase relative to the origin point  $C_1(0, c_1)$ , where  $c_1 = 0$ , is removed until the width of the tooth-like segment  $\Delta r(1, n_1)$  is larger than or equal to  $\Delta$  and  $\Delta r(1, n_1 + 1)$  is smaller than  $\Delta$ . The width of the  $n_1$ th tooth-like segment obtained from the first parabolic profile is

$$\begin{aligned} \Delta r(1, n_1) &= r(1, n_1) - r(1, n_1 - 1) \\ &= (2\lambda f n_1)^{1/2} - [2\lambda f (n_1 - 1)]^{1/2}, \end{aligned} \quad (3)$$

where  $r(1, n_1)$  is the position of the last tooth-like segment on the  $x$  axis. If even  $\Delta r(1, 1)$  is smaller than  $\Delta$ , let  $r(1, n_1) = 0$  and go to  $N = 2$  directly.

Second, let  $N = 2$  from point  $C_2[r(1, n_1), c_2]$  [black point in Fig. 1(a)], where  $c_2 = r(1, n_1)^2/(2\delta f \times 2)$ , and the profile of each parabolic lens changes to  $y_2 = x^2/(2\delta f \times 2)$ . The material causing a multiple of  $2\pi$  phase and an additional phase  $\varphi = 2\pi\delta c_2/\lambda$  relative to point  $O$  for each profile is removed. Then the total additional phase relative to the origin point  $\varphi_N$  ( $N = 2$ ) is

$$\varphi_N = N\varphi = 2 \frac{2\pi\delta r(1, n_1)^2}{\lambda \cdot 2\delta f \times 2} = 2\pi n_1, \quad (4)$$

which is also a multiple of  $2\pi$  and will not destroy the focusing. The removal will stop when  $\Delta r(2, n_2)$  is larger than or equal to  $\Delta$  and  $\Delta r(2, n_2 + 1)$  is smaller than  $\Delta$ . The width of the  $n_2$ th tooth-like segment obtained from the second parabolic profile is

$$\begin{aligned} \Delta r(2, n_2) &= [2\lambda f N_2 n_2 + 2\delta f N_2 c_2]^{1/2} \\ &\quad - [2\lambda f N_2 (n_2 - 1) + 2\delta f N_2 c_2]^{1/2}. \end{aligned} \quad (5)$$

If even  $\Delta r(2, 1)$  is smaller than  $\Delta$ , let  $r(2, n_2) = r(1, n_1)$  and go to  $N = 3$  directly.

The remainder can be done in the same manner with  $N$  increasing. As a result, the number of tooth-like segments obtained from the same profile will have the same group number  $N$ . All these tooth-like segments are rearranged regularly forming an X-ray focusing lens, shown in Fig. 1(b). The total additional phase difference caused by the material removed from the  $N_j$ th profile relative to the origin point  $O(C_1)$  is

$$\begin{aligned} \varphi_{N_j} &= N_j 2\pi \delta c_j / \lambda \\ &= 2\pi [N_{j-1} n_{j-1} + N_{j-2} n_{j-2} + \dots + N_1 n_1], \end{aligned} \quad (6)$$

where  $N$  and  $n$  are integers. The total additional phase differences are also an integer multiple of  $2\pi$ , which will not destroy the focusing. Therefore, the phase changes caused by the PL are the same as those caused by a PRL or KL with the same focal length.

### 2.2. Comparison with a compound KL

The total transmission  $T$  is defined as the ratio of the power incident on the lens to that behind the lens,

$$T = \frac{\int_{x_1}^{x_2} I_0(x) t(x) dx}{\int_{x_1}^{x_2} I_0(x) dx}, \quad (7)$$

where  $I_0(x)$  is the intensity distribution of the X-rays incident on the whole aperture of the lens,  $x_1 < x < x_2$ ,  $t(x) = \exp[-\mu f(x)]$  is the intensity transmission function through the lens,  $f(x)$  is the lens profile, and  $\mu$  is the total linear absorption coefficient. The effective aperture is defined as the width of slit that would transmit an equal amount of power (Lengeler *et al.*, 1999), which is the integration of the transmission function  $t(x)$  throughout the whole lens aperture  $x_1 < x < x_2$ ,

$$A_{\text{eff}} = \int_{x_1}^{x_2} t(x) dx. \quad (8)$$

Under the condition of the same fabrication capacity, *i.e.* the smallest segment width  $\Delta$  that can be successfully fabricated, when a compound KL (CKL) and a PL have the same focal length  $f$  and geometrical aperture  $A_g$ , the number of the outermost group of tooth-like segments  $N_{\text{out}}$  of the PL equals the group number of the CKL  $N$ . There are fewer tooth-like segments of the PL in the middle than the CKL, which leads to the fact that the whole transmission  $T$  and the effective aperture of the PL are larger than those of the CKL.

A numerical example is taken to show comparisons of the total transmission  $T$  and the effective aperture  $A_{\text{eff}}$  of a PRL, CKL and PL with the same focal length  $f = 3$  m, geometrical aperture  $\simeq 1.77$  mm and smallest segment width  $\Delta = 10 \mu\text{m}$ , and these lenses are all made of nickel working at 50 keV. The group number of the CKL  $N = 119$ , and the number of the outermost group of the PL  $N_{\text{out}} = 119$ . Results are shown in Table 1. Obviously, when these lenses have almost the same geometrical aperture, the effective aperture of the PL is 537.0  $\mu\text{m}$  which is two times larger than 246.1  $\mu\text{m}$  of the CKL and almost seven times larger than 77.8  $\mu\text{m}$  of the PRL.

Fig. 2 shows intensity profiles at the focal length of the CKL and the PL mentioned above when the incident light is a plane wave, which are simulated by the Fresnel–Kirchhoff integral (Born & Wolf, 1999). The PL realises good focusing in theory, and the maximum intensity at the focus of the PL is 3.3 times higher than that of the CKL.

Fig. 3 shows the relationship between the geometrical and effective aperture at different fabrication limits  $\Delta$ . For a fixed fabrication limit, the geometrical aperture of the PL can be enlarged by adding more tooth-like segments on two sides,

**Table 1**

Comparisons of the effective aperture and total transmission of the PRL, CKL and PL with the same geometrical aperture (@50 keV,  $f = 3$  m and  $\Delta = 10 \mu\text{m}$ ).

	PRL	CKL	PL
Geometrical aperture ( $\mu\text{m}$ )	1772.6	1765.2 <sup>†</sup>	1772.6
Effective aperture ( $\mu\text{m}$ )	77.8	246.1	537.0
Transmission	0.8%	13.9%	30.3%

<sup>†</sup> The geometrical aperture of the CKL is slightly different from the PRL and PL because of the limitation of  $\Delta = 10 \mu\text{m}$ .

leading to the enlargement of the effective aperture. Moreover, when the fabrication limit  $\Delta$  is decreased, the effective aperture of the PL will be larger for a constant geometrical aperture, which implies the focusing performance of the lens will be improved with the progress of the fabrication technology. The parameters for nickel material used in simulations are as follows:  $\delta = 7.07395 \times 10^{-7}$  and  $\mu = 22.0178 \times 10^{-4} \mu\text{m}^{-1}$  at 50 keV.

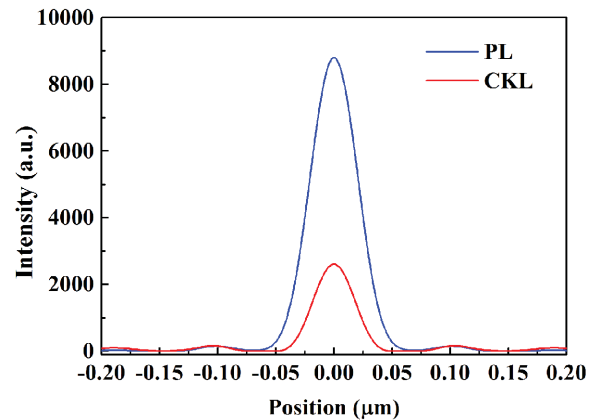


**Figure 2**

Intensity profiles at the focal length of the CKL and PL with the same aperture ( $f = 3$  m;  $\Delta = 10 \mu\text{m}$ ; aperture: 1.7 mm; working energy: 50 keV; material: nickel).

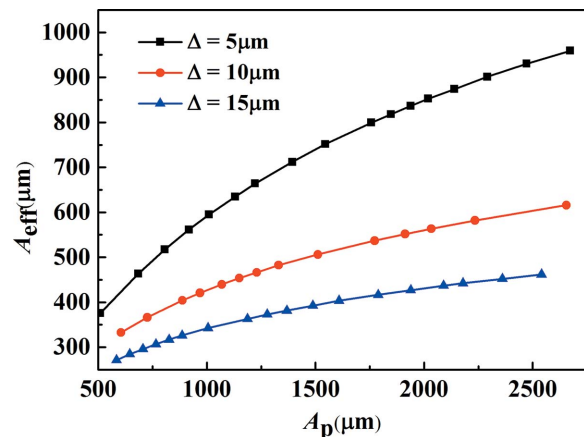


**Figure 3**

Relationship between the geometrical and effective aperture for different fabrication limitations  $\Delta$  ( $f = 3$  m; working energy: 50 keV; material: nickel).

**Table 2**  
Fabrication parameters of PLs (at 50 keV).

$f$ (m)	$\Delta$ ( $\mu\text{m}$ )	$h$ ( $\mu\text{m}$ )	$N_{\text{out}}$	Total $N$	$A_g$ (mm)	$L$ (mm)
3	10	30.05	119	5280	1.77	15

### 3. Fabrication

The fabricated parameters of the prototype PLs are listed in Table 2. The focal length  $f = 3$  m, and these lenses work at an X-ray energy of 50 keV; the smallest width of the tooth-like segment  $\Delta = 10 \mu\text{m}$ ; the length of every tooth-like segment  $h = 30.05 \mu\text{m}$ ; the lenses are composed of 5280 tooth-like segments and the outermost number  $N_{\text{out}}$  is 119; the whole geometrical aperture  $A_g$  is 1.77 mm and the total length  $L$  is about 15 mm.

The lenses are fabricated by LIGA technology (Bacher *et al.*, 1998; Nazmov *et al.*, 2005). The ‘fern-like’ profile, where even (or odd) segments are inverted (Snigireva *et al.*, 2001), is used to reduce the fabrication difficulties. The main fabrication processes are as follows. Firstly, an intermediate gold mask of thickness 1.2  $\mu\text{m}$  is fabricated by means of ultraviolet lithography technology and Au electroplating. Secondly, a working mask with a thick gold absorber of 12  $\mu\text{m}$  is formed using soft X-ray lithography and the intermediate mask. Thirdly, deep X-ray lithography with the use of a working X-ray mask and a harder X-ray spectrum compared with that used in the second step is carried out. After the development, PMMA structures with 250–400  $\mu\text{m}$  depth are obtained. Finally, after electroplating nickel, removing PMMA and polishing, the lens structures are attained.

Lens structures are studied using the scanning electron microscope (SEM). The SEM images of partial lenses are shown in Fig. 4. The width of the narrowest part of the tooth-

like segment is about 4  $\mu\text{m}$ . Fig. 4(a) shows that the tooth-like segments in the middle part of the lens have a translation along the propagation direction of X-rays, which is designed to avoid the PMMA structures falling down in the third step of the fabrication. The translation does not influence the focusing. In order not to disturb the phase changes caused by the lens, the bridge which can stabilize the whole structure (Cederström *et al.*, 2005; Nazmov *et al.*, 2005) is not introduced, clearly shown in Fig. 4(b), which unfortunately leads to about 10% of the tooth-like segments falling down. The fallen down segments are missing in the propagation trajectory of the X-rays shown in Figs. 4(a) and 4(d), and lie on the substrate shown in Figs. 4(a) and 4(c), which will not refract the X-rays to a desired direction and worsen the focusing.

### 4. Measurements

The focusing experiment was carried out at X-ray Imaging and Biomedical Application beamline BL13W1 at the Shanghai Synchrotron Radiation Facility, which has a wiggler source and operates at 3.5 GeV. The polychromatic radiation delivered by an eight-period wiggler was collimated by a mirror, and then monochromated to 50 keV by a Si (311) crystal monochromator in Laue geometry with an energy resolution of about  $10^{-3}$  keV. The effective source size is about 370  $\mu\text{m}$  (FWHM) in the horizontal and 23  $\mu\text{m}$  (FWHM) in the vertical. The tested lens was placed 33 m from the source and was focusing in the vertical direction. Alignment of the lens was performed using an X-ray CCD camera with 3.25  $\mu\text{m}$  pixel-size, which was also used for measurements. Moreover, a tantalum knife-edge was used for high-resolution beam profiles. The knife-edge was placed on a stage with the required rotation/translation degrees of freedom and was aligned with the X-ray CCD camera.

All the measurements presented here were made at an X-ray energy of 50 keV, and the lens under test is depicted in Fig. 4. Using the CCD camera, the narrowest focal line was found at a distance of about 3.3 m from the lens. The demagnification factor is 11:1 and the theoretical width of the focal line is 2.3  $\mu\text{m}$  (FWHM). The photon flux gain  $G$  is defined as the ratio of the photon flux in the size of the FWHM of the focal spot with lens to that without lens, giving a theoretical gain  $G = 159$ . The intensity map in the focal plane is shown in Fig. 5(a). The focal line has a width of 16.2  $\mu\text{m}$ , which is significantly larger than the theoretical one. The ratio of the peak intensity to the background is 9.5. The photon flux gain  $G$  is 7.2, substantially lower than that expected from theory. These can be partly explained by the insufficient resolution of the CCD camera.

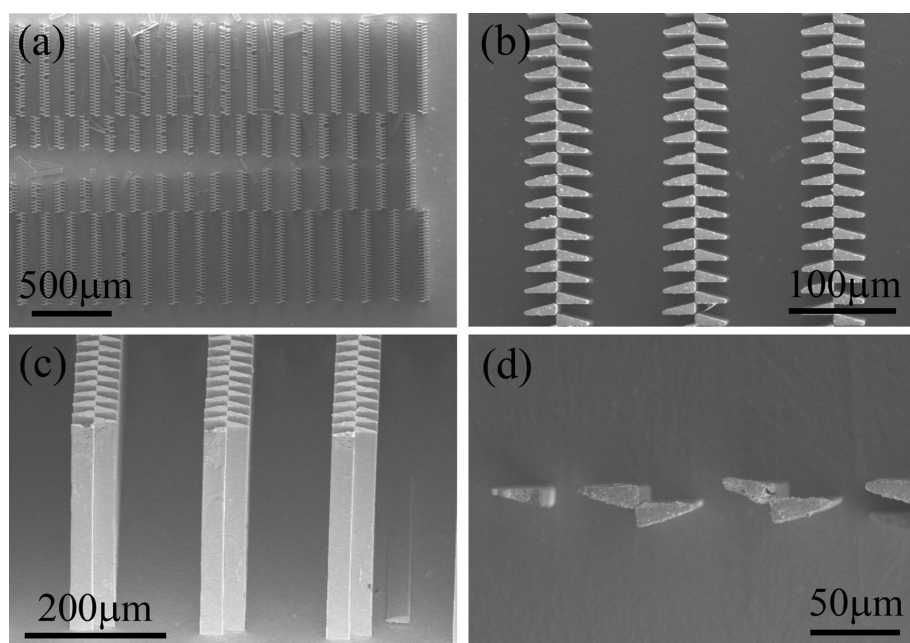


**Figure 4**  
SEM image of the PL produced by LIGA technology.

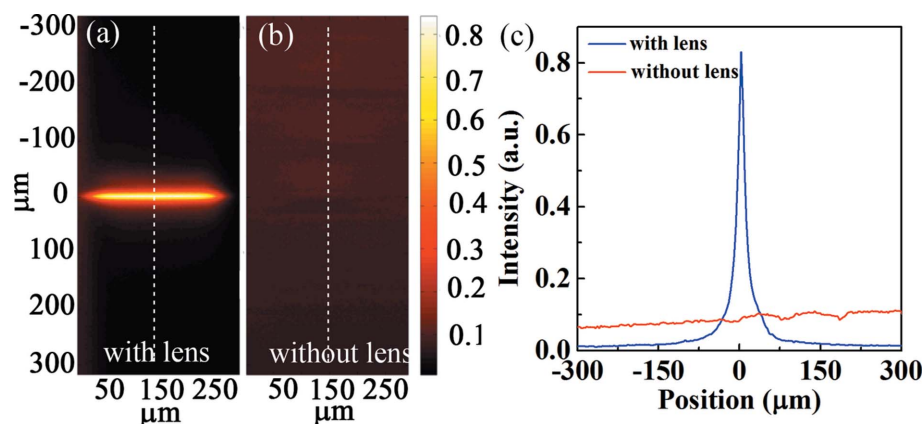


**Figure 5**  
Images with (a) and without (b) lens in the focal plane captured by a CCD camera. (c) Intensity profiles of the focused X-ray beam.

The result of a knife-edge scan of the focal line is shown in Fig. 6. With the improved resolution, the width of the focal line is measured to be  $7.7\ \mu\text{m}$ , and the photon flux gain  $G$  is about 14. It is noticed that the width of the focal line is still larger than the theoretical one, and the gain is lower than the theoretical value. The major impact on the broadened focal line and reduction in gain arises from the imperfection of the fabrication, such as the 10% of tooth-like segments falling down, the narrowest parts of the tooth-like segments not being sharp but round, and lens profiles and side-walls not being ideally perfect, as shown in Fig. 4. Furthermore, the knife-edge used in the experiment of poor quality would also enlarge the measurement result of the focal width. Finally, the thin-lens approximation is introduced without considering geometric scattering in the lenses (Nillius, 2012) and the edge diffraction effect of a tooth-like segment (Nazmov *et al.*, 2013), which lead to efficiency losses.

## 5. Conclusion

It has been shown that a prism-array X-ray lens can be obtained from different parabolic profiles with different parameters, the phase changes for a plane wave caused by

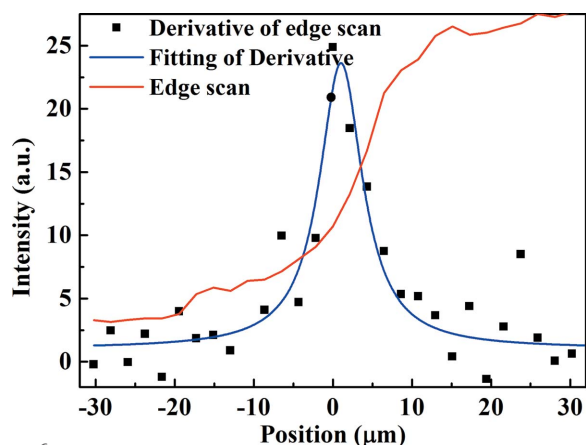


**Figure 6**  
Intensity profile in the focal plane measured with knife-edge scan.

which are accurately the same as those caused by a parabolic lens without any additional corrections. Its transmission and effective aperture are larger than those of the CKL with the same aperture and smallest width of the tooth-like segment. The aperture of this lens is not limited by the smallest width of the tooth-like segment that can be successfully fabricated within the tolerance of the state-of-the-art production technology. This design allows short focal lengths and high X-ray energy while preserving the feature size of the lens. The nickel lens made by LIGA with  $1.77\ \text{mm}$  aperture and about  $400\ \mu\text{m}$  depth provided a focal line width of

$7.7\ \mu\text{m}$ . Fabrication imperfections and poor quality of knife-edge broadened the focal width and limited the flux gain to 14 for one-dimensional focusing. In the future, we will improve the fabrication process to enhance the focusing gain, especially to avoid tooth-like segments breaking down. Actually, although nickel is not quite suitable for an energy of  $50\ \text{keV}$  but for higher energy ( $>80\ \text{keV}$ ), the paper demonstrates a new design for the prism-array lens which acts better than the traditional kinoform lens, and this design can be introduced either to light materials for lower energy or to heavy materials for higher energy. The prism-array lens with micro-focusing at high X-ray energy has great potential in micro-diffraction mapping techniques like near-field high-energy diffraction microscopy (Suter *et al.*, 2006) and pair distribution function measurements at high pressure using a diamond anvil cell (Hong *et al.*, 2016), *etc.*

## Acknowledgements

We gratefully thank staff at Beijing Synchrotron Radiation Facility for the fabrication of the lens and help in the experiment, and staff at Shanghai Synchrotron Radiation Facility for assistance in using beamline BL13W1. This work was supported by project 11305202 supported by NSFC.

## References

- Aristov, V., Grigoriev, M., Kuznetsov, S., Shabelnikov, L., Yunkin, V., Weitkamp, T., Rau, C., Snigireva, I., Snigirev, A., Hoffmann, M. & Voges, E. (2000). *Appl. Phys. Lett.* **77**, 4058–4060.
- Bacher, W., Bade, K., Matthis, B., Saumer, M. & Schwarz, R. (1998). *Microsystem Technol.* **4**, 117–119.
- Born, M. & Wolf, E. (1999). *Principles of Optics*. Cambridge University Press.
- Cederström, B., Ribbing, C. & Lundqvist, M. (2005). *J. Synchrotron Rad.* **12**, 340–344.
- Evans-Lutterodt, K., Ablett, J., Stein, A., Kao, C.-C., Tennant, D., Klemens, F., Taylor, A., Jacobsen, C., Gammel, P., Huggins, H., Bogart, G., Ustin, S. & Ocola, L. (2003). *Opt. Express*, **11**, 919–926.
- Evans-Lutterodt, K., Stein, A., Ablett, J., Bozovic, N., Taylor, A. & Tennant, D. (2007). *Phys. Rev. Lett.* **99**, 134801.
- Hong, X., Ehm, L., Zhong, Z., Ghose, S., Duffy, T. S. & Weidner, D. J. (2016). *Sci. Rep.* **6**, 21434.

- Jark, W., Pérennès, F., Matteucci, M., Mancini, L., Montanari, F., Rigon, L., Tromba, G., Somogyi, A., Tucoulou, R. & Bohic, S. (2004). *J. Synchrotron Rad.* **11**, 248–253.
- Lengeler, B., Schroer, C. G., Benner, B., Günzler, T. F., Kuhlmann, M., Tümmler, J., Simionovici, A. S., Drakopoulos, M., Snigirev, A. & Snigireva, I. (2001). *Nucl. Instrum. Methods Phys. Res. A*, **467–468**, 944–950.
- Lengeler, B., Schroer, C., Tümmler, J., Benner, B., Richwin, M., Snigirev, A., Snigireva, I. & Drakopoulos, M. (1999). *J. Synchrotron Rad.* **6**, 1153–1167.
- Nazmov, V., Mohr, J. & Simon, R. (2013). *J. Micromech. Microeng.* **23**, 095015.
- Nazmov, V., Reznikova, E., Snigirev, A., Snigireva, I., DiMichiel, M., Grigoriev, M., Mohr, J., Matthis, B. & Saile, V. (2005). *Microsyst Technol.* **11**, 292–297.
- Nillius, P. (2012). *AIP Conf. Proc.* **1437**, 111–115.
- Schroer, C., Kuhlmann, M., Hunger, U., Günzler, T., Kurapova, O., Feste, S., Frehse, F., Lengeler, B., Drakopoulos, M., Somogyi, A., Simionovici, A. S., Snigirev, A., Snigireva, I., Schug, C. & Schröder, W. H. (2003). *Appl. Phys. Lett.* **82**, 1485–1487.
- Simon, M., Reznikova, E., Nazmov, V., Last, A. & Jark, W. (2008). *Proc. SPIE*, **7077**, 70771Q.
- Snigirev, A., Kohn, V., Snigireva, I. & Lengeler, B. (1996). *Nature (London)*, **384**, 49–51.
- Snigirev, A., Kohn, V., Snigireva, I., Souvorov, A. & Lengeler, B. (1998). *Appl. Opt.* **37**, 653–662.
- Snigireva, I., Snigirev, A., Rau, C., Weitkamp, T., Aristov, V., Grigoriev, M., Kuznetsov, S., Shabelnikov, L., Yunkin, V., Hoffmann, M. & Voges, E. (2001). *Nucl. Instrum. Methods Phys. Res. A*, **467–468**, 982–985.
- Suter, R., Hennessy, D., Xiao, C. & Lienert, U. (2006). *Rev. Sci. Instrum.* **77**, 123905.